



Fluoride, iron and manganese removal from brackish groundwater by solar-powered vacuum membrane distillation

Ying Zhang^{a,*}, Muttucumaru Sivakumar^a, Mohammad Ramezani-pour^b,
Shuqing Yang^a, Keith Enever^c

^aSchool of Civil, Mining and Environmental Engineering, Faculty of Engineering and Information Sciences, University of Wollongong, Northfields Ave, Wollongong, NSW 2500, Australia, Tel. +61 450212385; email: yz393@uowmail.edu.au (Y. Zhang), Tel. +61 2 4221 3055; email: siva@uow.edu.au (M. Sivakumar), Tel. +61 2 4221 3070; email: shuqing@uow.edu.au (S. Yang)

^bDepartment of Engineering and Architectural Studies, Ara Institute of Canterbury, Madras St, Christchurch Central, Christchurch 8011, New Zealand, Tel. +64 3 940 8023; email: matt.pour@ara.ac.nz

^cSchool of Mechanical, Materials, Mechatronics and Biomedical Engineering, Faculty of Engineering and Information Sciences, University of Wollongong, Northfields Ave, Wollongong, NSW 2500, Australia, email: kenever@uow.edu.au

Received 28 March 2018; Accepted 18 August 2018

ABSTRACT

Investigations on a solar-powered vacuum membrane distillation (SVMD) system were conducted for removal of fluoride, iron and manganese from brackish groundwater. A commercial capillary membrane module with effective surface area of 0.1 m² was used in the SVMD system. Results showed that over 99% salt rejection rate and over 97% removal efficiency of fluoride, iron and manganese were achieved. Total dissolved solids of the permeate water were in the range of 1–10 mg/L while all contaminants concentrations were well below the World Health Organization drinking water guidelines. Condensation efficiency was found to have significant influence on the performance of the SVMD system. During Phase I of the study, the permeate pressure increased almost linearly with the membrane feed temperature due to insufficient condensation, which negatively affected the permeate flux. The highest permeate flux observed was 5.02 L/m² h on September 19th, 2016. The corresponding daily production and gain output ratio (GOR_{so}) were 2.17 L and 0.26, respectively. In Phase II, a new condenser was installed to enhance the condensation efficiency. Significant improvement of the permeate flux was obtained with the highest permeate flux being 8.84 L/m² h on November 5th, 2016. Consequently, much higher daily production (5.00 L) and GOR_{so} (0.40) were achieved.

Keywords: Solar energy; Vacuum membrane distillation; Groundwater; Fluoride; Iron and manganese

1. Introduction

Water stress has become one of the major problems faced by human society in this century. Worldwide freshwater demand keeps rising due to rapid population growth, urbanization and industrialization, while in contrast the availability of freshwater resources is decreasing in many regions of the world because of water pollution, overexploitation and

climate change. According to the United Nations [1], by 2025, 1.8 billion people will be living in countries or regions with absolute water scarcity and two-thirds of the world's population could be under water stress conditions. In order to alleviate water stress and enhance water security in the future, alternative water sources have to be considered for water supply. In recent years, brackish groundwater (BGW) is gaining increasing importance as a supplement or even replacement for freshwater resource in many countries including the United States, Spain, the Netherlands, Australia

* Corresponding author.

and in Middle Eastern Countries [2–7]. Considering the total dissolved solids (TDS) limit of 600 mg/L for palatability purposes in the World Health Organization (WHO) drinking water quality guideline, BGW can be regarded as groundwater having TDS ranging from 600 to 30,000 mg/L [8]. Moreover, the U.S. Environmental Protection Agency (EPA) has defined the TDS range of potential groundwater sources that can be considered for drinking water supply as less than 10,000 mg/L [9]. Desalination technologies must be adopted to remove the large amount of salt from BGW in order to meet the drinking water quality standard.

Besides the high salinity, BGW often contains some naturally occurring contaminants such as fluoride, iron and manganese. Strict regulations have been established on the levels of these contaminants due to health or aesthetic reasons. Fluoride in groundwater mainly originates from fluoride-containing minerals such as fluorite, sellaite and biotites [10,11]. Worldwide, its concentration in groundwater normally ranges from 0 to 10 mg/L. However, high concentrations of fluoride, up to more than 100 mg/L, also occur in some places due to discharge of fluoride-containing effluents during industrial activities [10]. Excess amount of fluoride intake can cause dental and skeletal fluorosis, or result in crippling fluorosis in the worst cases [12]. A concentration limit of 1.5 mg/L in drinking water is recommended by the WHO to avoid the harmful effects of fluoride on human health [8]. Iron and manganese are common elements found in the earth's crust. They frequently coexist in groundwater in the dissolved form of Fe(II) and Mn(II). Naturally, iron and manganese will be released into the aquifer while groundwater flows through soils and rocks that dissolve them. Besides, anthropogenic sources (e.g., industrial effluents, acid mine drainage, well casing, pump parts and piping) can also contribute to iron and manganese concentrations in groundwater [13]. Elevated levels of iron and manganese can make the water unsuitable for drinking water supply mainly due to aesthetic reasons, causing metallic taste, coloration, turbidity and staining problems [14]. The threshold values of iron and manganese in drinking water have been set by WHO at 0.3 and 0.1 mg/L, respectively [8]. Therefore, the capability of effectively removing these contaminants has to be examined in the evaluation of desalination technologies for supplying safe drinking water from BGW sources.

Membrane distillation (MD) is a thermally driven separation process featured by the utilization of porous hydrophobic membranes that only allow vapour molecules to pass through. Vapour pressure across the membrane is the driving force of this process. The liquid solution is kept at the feed side due to the hydrophobicity character of the membrane. MD has been widely accepted as an alternative desalination technology. Different configurations of MD have been developed, including four basic configurations (i.e., DCMD, direct contact membrane distillation; AGMD, air gap membrane distillation; VMD, vacuum membrane distillation and SGMD, sweeping gas membrane distillation) and a few newly developed ones such as multistage membrane distillation, PGMD (permeate gap membrane distillation), MGMD (material gap membrane distillation) and V-MEMD (vacuum multieffect membrane distillation) [15,16]. Compared with conventional thermal desalination technologies such as MSF (multistage flash distillation) and MED (multieffect distillation), MD

requires a relatively low operating temperature, normally between 40°C and 80°C, which makes it suitable to be combined with low grade heat, namely, solar energy, geothermal energy and industrial waste heat. In recent years, solar-powered membrane distillation has received increased global attention. Several demonstration plants have been built over the past decade. An autonomous solar VMD pilot plant was designed and implemented for seawater desalination in Mahares, Tunisia [17]. Flat plate solar collectors and photovoltaic (PV) panels are used to supply thermal and electrical energy to the system, respectively. Daily production of the plant was reported at 210 L/d. Raluy et al. [18] reported the 5-year operational experience of a 100 L/d solar membrane distillation demonstration plant located in Gran Canary Island, Spain. A solar MD experimental compact system based on a PGMD module developed by Fraunhofer ISE was adopted in the plant. During the 5 years operation, high-quality distillate with conductivity at 20–200 $\mu\text{S}/\text{cm}$ was produced with actual daily water production of 5–120 L/d. Chafidz et al. [19] developed a pilot autonomous solar MD system and it was tested for desalination of brackish water in Saudi Arabia. A novel memsys V-MEMD module was used in the system. Daily production ranging from 32.4 to 99.6 L/d was achieved at different weather conditions. Though being regarded as a promising solution for sustainable water supply in regions blessed with high solar radiation, solar membrane distillation is not commercialized yet. Major factors that constrained the commercialization of solar membrane distillation include the lack of commercially available high performance MD membranes with sufficient wetting resistance, the high energy consumption (specific thermal energy consumption reported as 100–1,000 kWh/m³) and the high water production cost (reported as US\$12–18/m³) which makes it less economically competitive with conventional desalination technologies based on fossil fuels [16,20]. Further development of low-cost high-performance MD membranes and energy efficient membrane modules, further solar MD modelling and application studies are required for the commercialization and scaling up of this technology.

A three-loop solar-powered vacuum membrane distillation (SVMD) system has been developed in this study. It was designed to be operated autonomously when there is abundant solar radiation. Evacuated tube solar collectors and PV panels are utilized to supply thermal and electrical energy, respectively. A commercial polypropylene capillary membrane module is adopted in the VMD process. VMD was selected because it has the potential to obtain relatively higher permeate flux at the same feed temperature among the four basic configurations due to increased vapour pressure difference caused by the applied vacuum at the membrane permeate side [21]. Extensive studies of seawater and brackish water desalination with MD have been conducted by researchers. However, very few investigations focused on the removal of specific contaminants in BGW. Fluoride removal from BGW has been investigated by Yarlagadda et al. [12] and Hou et al. [22] using DCMD. The highest fluoride concentration observed in the permeate water was found to be 0.56 mg/L [12], far below the drinking water standard. In the study of Hou et al. [22], fluoride concentrations in the permeate all fell below the detection limit of their instrument. So far, VMD has not been reported for fluoride

removal from BGW. The removal of iron and manganese from groundwater with MD was also absent in the literature. The objective of this study is to demonstrate the feasibility of drinking water production from BGW with SVMMD as well as examine the removal efficiency of fluoride, iron and manganese. The experiments were conducted under real weather conditions. The dynamic daily performance of the SVMMD system is also presented and discussed.

2. Experimental

2.1. Experimental setup

A three-loop standalone solar powered vacuum membrane distillation (SVMD) experiment setup was designed and constructed in this study (Fig. 1). Three major components in the setup include: the VMD system, the solar thermal system and the solar PV electricity supply system. Besides, online monitoring devices were installed in the system for data acquisition purposes. As shown in Fig. 1, there are three water loops in the SVMD system: the first loop is the solar heating loop in which tap water circulates as heat transfer fluid in the solar thermal system, the second loop is the membrane feeding loop in which the feed water circulates through the membrane module and the third loop is the condensation loop in which the cooling water flows through the condenser to condense the produced vapour at the permeate side of the membrane module.

The solar thermal system provides thermal energy to heat up the feed water in the hot water storage tank. A 16-tube evacuated tube collector with 1.33 m² aperture area is used to capture and convert solar energy. Clean tap water

is circulated in the solar thermal cycle as the heat transfer liquid. Feed water for the VMD system is heated up by the heat transfer liquid in a 14 L insulated storage tank via a copper coil heat exchanger. A 50 L buffer tank was installed in the solar thermal system to supply makeup water to the cycle as well as to store surplus energy on hot summer days.

The solar PV system provides electricity to operate all the electrical equipment including pumps, sensors, laptop and other monitoring devices. It consists of two PV panels with peak power of 210 W each, a charge controller, two 12 V-60 AH deep cycle batteries and a DC/AC inverter. The electricity is directly supplied from the batteries in order to have stable voltage. The total electrical load of the pumps and monitoring devices is about 300W during the regular operation time in this study. The system could work independently on sunny days. In cloudy weather, extra electricity from the grid will be needed.

The VMD system consists of a membrane module, a condenser, an evaporative cooling device, a vacuum pump, two circulating pumps, a 14 L hot (feed) water storage tank, a 15 L permeate water tank and a 30 L cooling water tank. A commercial polypropylene capillary module MD020CP2N, purchased from Microdyn (Germany) was used for BGW desalination in this study. It contains 40 fibres with an effective membrane area of 0.1 m².

In the first phase of this study (fluoride removal experiments), a jacketed coil glass condenser (Fig. 1) CX6/33/SC manufactured by QUICKFIT (UK) was utilized for condensing the permeate vapour from the membrane module. The condenser has an approximate surface area of 400 cm² and an effective length of 160 mm. Later, to enhance the condensation efficiency, a new shell-and-tube condenser has been

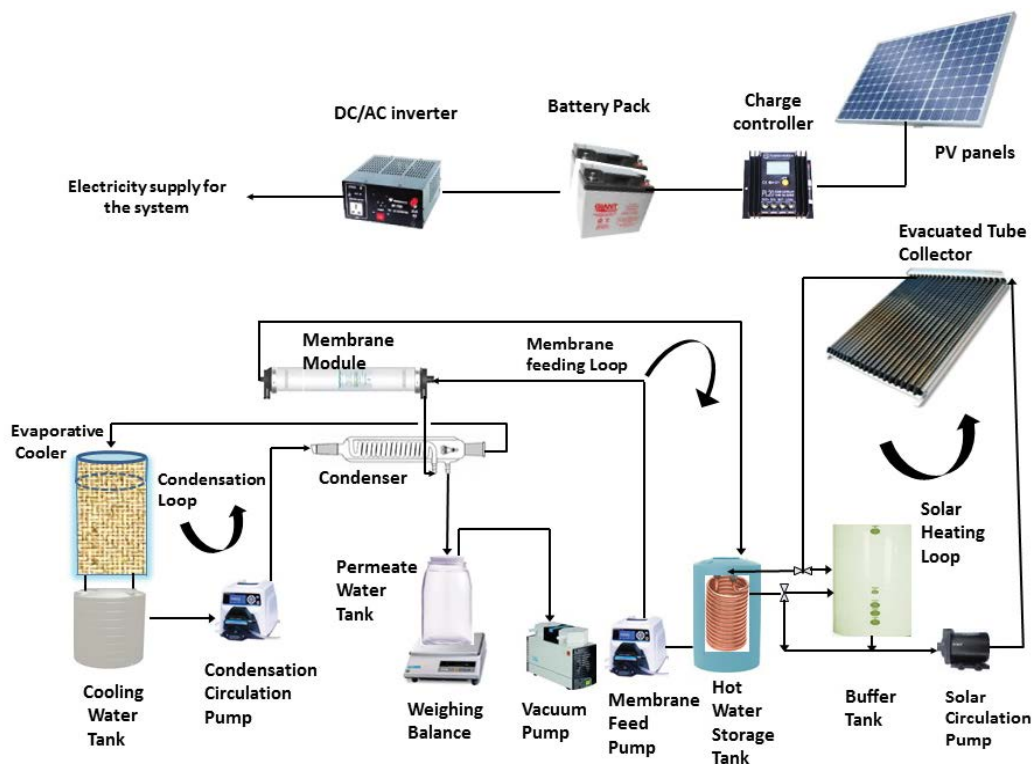


Fig. 1. Schematic diagram of SVMMD experimental setup.

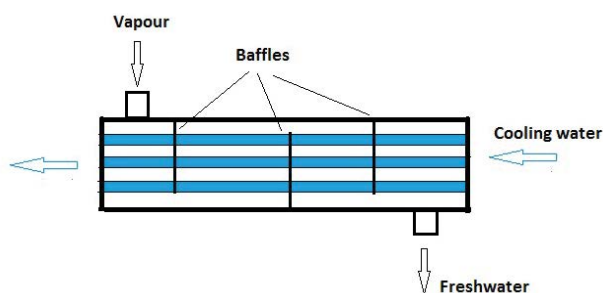


Fig. 2. Schematic diagram of the shell-and-tube condenser.

designed and installed to replace the initial glass condenser (Fig. 2). It consists of a copper shell and 31 copper tubes with inner diameter 4.35 mm and total length of 400 mm. Cooling water flows through the copper tube while vapour passes through the shell side. Three baffles were installed along the vapour path to ensure adequate retention time of the vapour and avoid short flow. The second phase of this study (iron and manganese removal experiments) was conducted with the new condenser.

An evaporative cooling device was built to cool down the circulating cooling water after condensation. The cooling water is distributed to a cylindrical dish and then trickles down to the cooling water tank through the surrounding burlap fabrics. The water is cooled down by heat transfer with the air as well as by evaporation. The heat transfer area of the burlap is about 0.5 m². An N840.3FT.18 Javac KNF laboratory vacuum pump was used to create vacuum pressure in the permeate side. The pump can reach a lowest absolute pressure of 0.8 kPa. Two Masterflex peristaltic pumps were used to circulate the feed water through the membrane module (capacity 0–2.0 L/min) and to circulate the cooling water (capacity 0–0.4 L/min), respectively. In the second phase of the study, a new submerged cooling water circulation pump with higher capacity (0–4.0 L/min) was installed to work together with the new condenser.

An online monitoring system was established in the SVMD setup. Operating parameters such as temperatures, permeate pressure and permeate water weight, as well as meteorological data (including solar radiation, air temperature, humidity, wind speed and direction), were all recorded by online sensors or devices and transferred to a LabVIEW(2013) program in the PC via data loggers.

2.2. Material and methods

Experiments were conducted with SVMD to treat synthetic BGW containing fluoride, iron and manganese. The synthetic BGW was prepared using analytical grade chemicals and deionized water (Milli-Q system). The composition of the synthetic water was determined based on BGW properties from the literature. The proportions of major ions in BGW were summarized and presented in Table 1. The chemical recipe of synthetic BGW was made based on Table 2. Fluoride, iron and manganese were spiked in the synthetic water with NaF, Fe₂SO₄ · 7H₂O and MnCl₂ · 4H₂O, respectively.

The experiments were carried out in two phases: Phase I, fluoride removal experiments with a glass condenser in SVMD; Phase II, iron and manganese removal experiments

Table 1
Proportion of major ions in brackish groundwater from the literature

Ions	Proportion (wt%)
Na	10–31
K	0.4–1.5
Ca	1.1–14
Mg	2–6.2
Cl ⁻	7–49
SO ₄ ²⁻	0.9–40
HCO ₃ ⁻	0.9–12
NO ₃ ⁻	0.0–8.6

Note: The ion proportions are summarized from the literature [4,7,12,23–29].

Table 2
Synthetic brackish groundwater recipe

Chemicals	Proportion in TDS (wt%)
NaCl	50.0
Na ₂ SO ₄	18.0
KCl	2.0
CaCl ₂	16.0
MgCl ₂	8.0
NaHCO ₃	3.0
NaNO ₃	3.0

with a shell-and-tube condenser in SVMD. In each phase, there are two groups of experiments. The first group was conducted by feeding TDS 2,000 mg/L synthetic water spiked with a range of fluoride (2–100 mg/L) or iron/manganese concentrations (Fe²⁺, 1–10 mg/L; Mn²⁺, 1–5 mg/L). In the second group, feed water TDS varied from 2,000 to 10,000 mg/L while fluoride or iron/manganese concentrations were fixed (F⁻, 10 mg/L; Fe²⁺, 10 mg/L; Mn²⁺, 2 mg/L).

All the tests were conducted under real weather conditions in a partly shaded yard on the main campus of the University of Wollongong, NSW, Australia. Real-time data (temperatures, permeate pressure, permeate water weight and meteorological data) were monitored and recorded during the operation of the SVMD system. Permeate water samples were taken at the end of each day for water quality measurement. The TDS concentration of the permeate water was determined by measuring the conductivity of the water sample with a multiparameter water quality meter Eutech Instrument PCD 650. Iron and manganese concentrations were analysed with inductively coupled plasma optical emission spectrometry (Agilent 710 ICP-OES). A Shimadzu Ion Chromatography unit equipped with a Dionex Ion Pac AS23 column was used to measure fluoride concentration.

3. Results and discussion

3.1. Fluoride removal tests

The fluoride removal experiments were carried out during September 2016 under real weather conditions. A total of 10

tests were conducted with different feed water TDS and feed fluoride concentrations. Each test was done in a single day from 9:00 to 16:00 (during the tests period, little solar radiation is available in the location of the SVMMD setup after 15:30). In all the tests, the feed water flow rate was kept at 1.22 L/min (corresponding to a 0.2 m/s feed side velocity along the membrane fibres). Meanwhile, 0.3 L/min cooling water flow rate and 1.5 L/min water circulation rate at the solar cycle was used. The vacuum pump was operated to its full capacity. However, the permeate side pressure could hardly be kept constant which will be discussed in detail in Section 3.1.2. At the start of each day, 10 L feed water was manually fed into the hot water storage tank. Permeate water samples were taken at the end of day.

3.1.1. Fluoride removal and salt rejection rates

The first six tests were conducted with feed water TDS 2,000 mg/L and F⁻ concentration 2, 5, 10, 20, 50 and 100 mg/L, respectively. The remaining four tests were conducted with F⁻ concentration 10 mg/L and TDS 4,000, 6,000, 8,000 and 10,000 mg/L, respectively. The conductivity and fluoride in the permeate water were tested.

The results are shown in Table 3. The salt rejection rate or fluoride removal efficiency of the membrane was calculated using the following equation:

$$R(\%) = \frac{C_f - C_p}{C_f} \times 100\% \quad (1)$$

where C_f is the TDS/ F⁻ concentration in the feed water and C_p is the TDS/ F⁻ concentration in the permeate water.

In all the tests, fluoride was effectively removed. Its concentrations in the permeate water samples were all below the detection limit of the instrument which is 0.05 mg/L. The removal efficiency was above 97.5%. Meanwhile, more than 99.8% of salt was removed during the process. Good quality permeates with TDS less than 7 mg/L were achieved in the tests. No remarkable effect of feed water salt concentration was shown on permeate water quality (Fig. 3). Only slightly

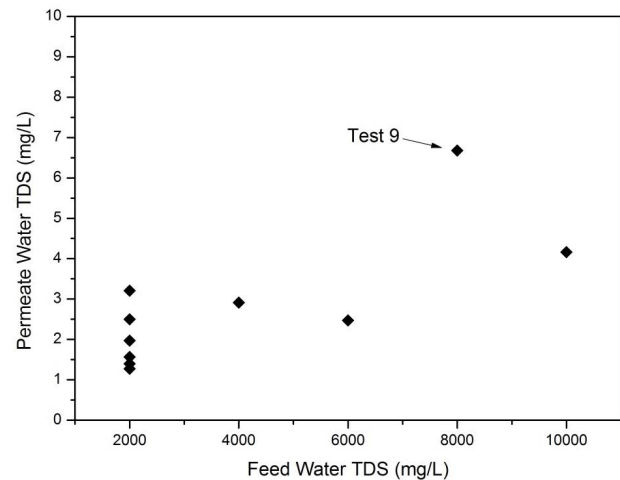


Fig. 3. Variation of permeate water TDS with different feed water salt concentrations (Phase I).

higher permeate TDS was obtained in the last two tests in the case of 8,000 and 10,000 mg/L feed TDS. The highest permeate TDS obtained in the ninth test could have been due to the long interval (5 d) between tests. Further discussion is presented in Section 3.2.1.

3.1.2. SVMMD daily performance

Highest daily permeate water production (2.17 L) was obtained on September 19th (Test 9). The daily performance of the SVMMD system on that day is presented in Fig. 4. The figure reflects the variation of operating conditions (solar radiation, air temperature, membrane feed temperature, permeate pressure and condenser inlet/outlet temperature) and permeate production during the day. The membrane permeate fluxes were average values calculated every half hour.

As shown in Fig. 4, effective solar radiation (> 400 W/m²) was obtained between 9:30 and 15:30. It reached the peak (810 W/m²) at around 12:00. Membrane feed temperature

Table 3
Permeate water quality during fluoride removal experiments

Test	Date	Feed TDS (mg/L)	Feed F ⁻ (mg/L)	Permeate conductivity (μS/cm)	Permeate TDS ^a (mg/L)	Salt rejection rate (%)	Permeate fluoride (mg/L)	F ⁻ removal efficiency (%)
1	Sep. 5th	2,000	2	2.40	1.27	99.9	<0.05 ^b	>97.5
2	Sep. 6th	2,000	5	3.72	1.97	99.9	<0.05	>99.0
3	Sep. 9th	2,000	10	4.72	2.50	99.9	<0.05	>99.5
4	Sep. 12th	2,000	20	2.64	1.40	99.9	<0.05	>99.8
5	Sep. 15th	2,000	50	6.05	3.21	99.8	<0.05	>99.9
6	Sep. 16th	2,000	100	2.96	1.57	99.9	<0.05	~100
7	Sep. 19th	4,000	10	5.50	2.92	99.9	<0.05	>99.5
8	Sep. 20th	6,000	10	4.66	2.47	~100	<0.05	>99.5
9	Sep. 26th	8,000	10	12.6	6.68	99.9	<0.05	>99.5
10	Sep. 27th	10,000	10	7.85	4.16	~100	<0.05	>99.5

^aTDS in the permeate water was calculated by '0.53*Conductivity'. The correlation factor 0.53 was determined by experiment.

^b0.05 mg/L is the fluoride detection limit of the instrument used.

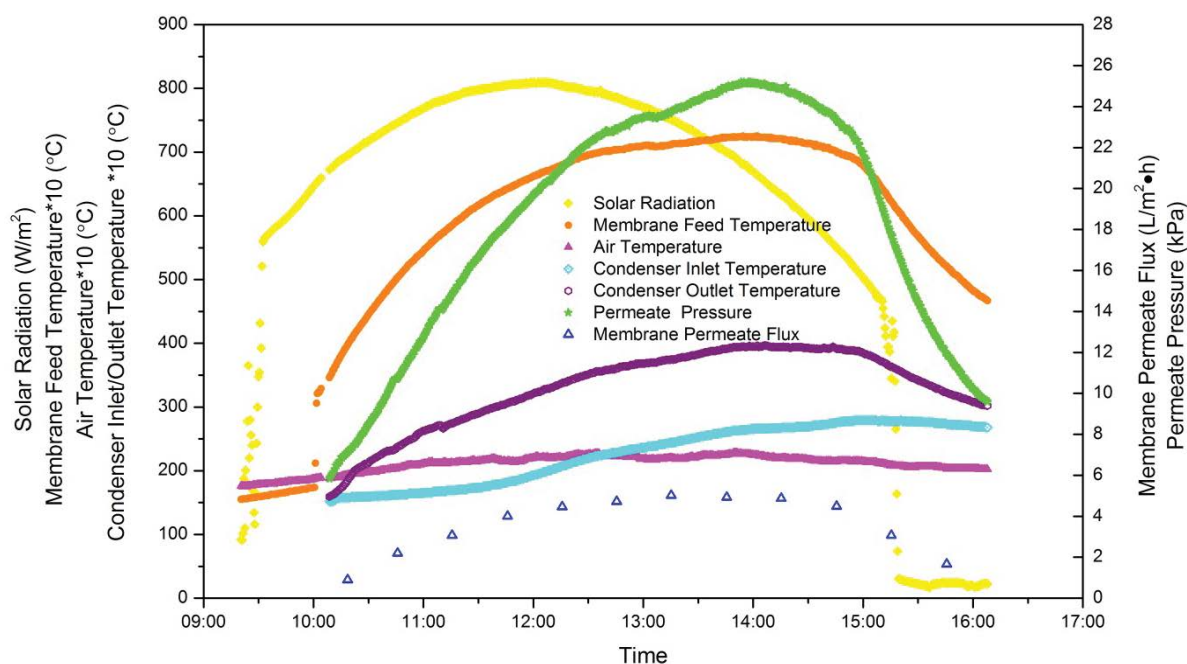


Fig. 4. Performance of the SVMD on September 19th, 2016. Variation of solar radiation, W/m^2 ; air temperature, $^{\circ}\text{C}$; membrane feed temperature, $^{\circ}\text{C}$; condenser inlet temperature, $^{\circ}\text{C}$; condenser outlet temperature, $^{\circ}\text{C}$; permeate pressure, kPa and membrane permeate flux, $\text{L}/\text{m}^2\cdot\text{h}$.

increased gradually with the accumulation of incident solar energy. The highest temperature 72.5°C occurred at around 14:00. Relatively stable membrane feed temperature was kept at noon. The variation of permeate flux was similar to membrane feed temperature. The peak average flux $5.02 \text{ L}/\text{m}^2\cdot\text{h}$ was achieved between 13:00 and 13:30. The corresponding average membrane feed temperature and permeate pressure were 71.2°C and 23.8 kPa , respectively. With the production of permeate water, the condenser inlet cooling water temperature gradually increased from 15.2°C to 27.9°C . This indicates that the heat loss through the evaporative cooling device was less than the energy gained from condensation of the produced vapour. It could also be noticed that the temperature differences between the condenser inlet and outlet cooling water temperature were relatively constant (around 13°C) from 12:00 to 15:00, when the membrane permeate flux was the highest of the day. This phenomenon was correlated with the relatively stable permeate flux during this period.

Dramatic variation of permeate side pressure was observed during the SVMD operation. An almost linear relationship was present between the membrane feed temperature and permeate pressure (Fig. 5) especially when the temperature was above 45°C . Starting from less than 6 kPa , it reached as high as 25 kPa around 14:00. The increased permeate pressure significantly reduced the driving force of membrane distillation at higher temperature and consequently limited the obtained permeate flux. After investigation, it was discovered that the increased permeate pressure was mainly caused by inadequate condensation of the produced vapour which accumulated between the membrane outlet and the glass condenser. To increase the efficiency of the condensation system, a new condenser was designed and constructed for the next phase of experiments

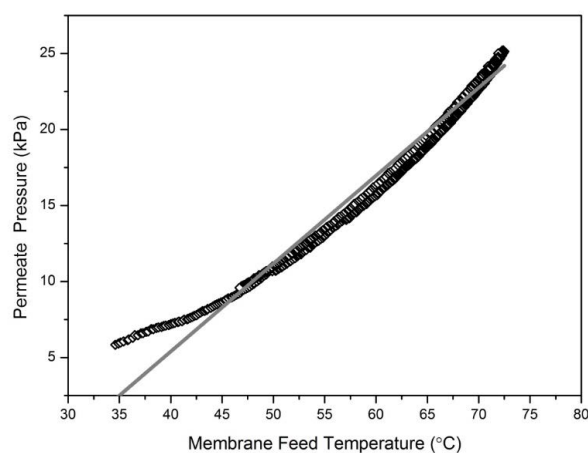


Fig. 5. Variation of permeate pressure with the change of membrane feed temperature (September 19th).

(as outlined in Section 2.1). A new cooling water circulation pump with higher capacity was also installed.

3.1.3. Production and thermal efficiency of the SVMD system

During these 10 tests, the daily production of the system was in the range of $1.00\text{--}2.17 \text{ L}$. As shown in Fig. 6, the variation of daily production was in accordance with the variation of daily solar radiation levels. The overall thermal efficiency of the system could be represented by GOR_{so} (gain output ratio-solar), which is defined as the energy ratio of total latent heat of produced distillate to the total incident solar energy [20]. It was calculated with the following equation:

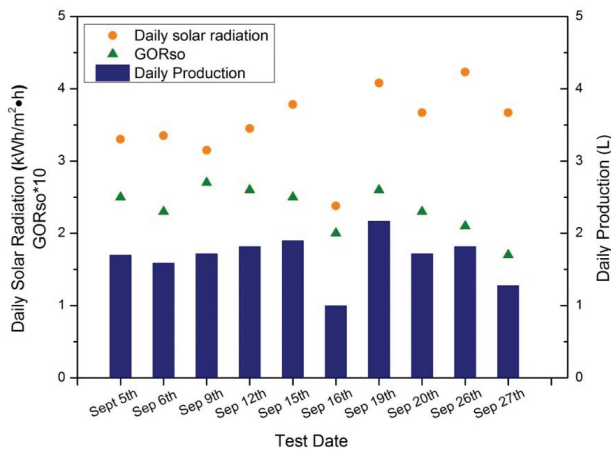


Fig. 6. Daily solar radiation, permeate production and thermal efficiency on different test days (Phase I).

$$GOR_{SO} = \frac{m_d \times \Delta H_v}{3600 \times A_a \times G} \quad (2)$$

where m_d is the daily distillate mass production (kg/d), ΔH_v is the latent heat for evaporation (kJ/kg), A_a refers to the aperture area of the solar collector and G is the daily solar radiation (kWh/m²·d).

The GOR_{so} of the SVM D system varied between 0.17 and 0.27, indicating the thermal efficiency of this system was quite low.

3.2. Iron and manganese removal tests

The iron and manganese removal experiments were carried out during October and November 2016 after the

installation of the new condenser and cooling water circulation pump. A total of 13 tests were conducted with different feed water TDS and feed iron/manganese concentrations. Each test was done in a single day from 9:30 to 17:30 (it was during daylight saving time). During all the tests, the feed water flow rate was kept at 1.22 L/min. Meanwhile, 2 L/min cooling water flow rate and 1.5 L/min water circulation rate at the solar cycle was used. The vacuum pump was operated to its full capacity. 12 L feed water was manually fed into the hot water storage tank at the start of each day. Permeate water samples were taken at the end of day.

3.2.1. Iron/manganese removal and salt rejection rates

The first nine tests were conducted with feed water TDS 2,000 mg/L and various Fe²⁺ and Mn²⁺ concentrations (Table 4). As iron and manganese often coexist in groundwater, Fe²⁺ only, Mn²⁺ only and Fe²⁺/Mn²⁺ both added conditions were all included in the tests. The remaining four tests were conducted with 10 mg/L Fe²⁺, 2 mg/L Mn²⁺ and TDS 4,000, 6,000, 8,000 and 10,000 mg/L, respectively. The conductivity and iron/manganese concentration in the permeate water were tested. Results are shown in Table 4. The removal efficiency of iron and manganese was also calculated by equation (1) with C_f and C_p referring to the concentration of iron/manganese in the feed and the permeate water, respectively.

Iron and manganese concentrations in the permeate water were all below the limit set in the WHO drinking water guideline [8]. As shown in Table 4, more than 97.4% of iron and more than 99.7% of manganese were removed. No obvious effects of the feed and iron/manganese concentrations were found on their concentrations in the permeate water. Iron was detected in the permeate water sample in the second test when there was no Fe²⁺ spike in the synthetic groundwater, which indicates that the iron in the permeate water

Table 4
Permeate water quality during iron/manganese removal experiments

Test	Date	Feed TDS (mg/L)	Feed Fe ²⁺ (mg/L)	Feed Mn ²⁺ (mg/L)	Permeate conductivity (μS/cm)	Permeate TDS ^a (mg/L)	Salt rejection rate (%)	Permeate Fe (mg/L)	Fe removal efficiency (%)	Permeate Mn (mg/L)	Mn removal efficiency (%)
1	Oct. 21th	2,000	0	1	3.50	1.82	99.9	^b <0.0050	NA ^d	0.0007	99.9
2	Oct. 24th	2,000	0	2	2.90	1.51	99.9	0.0120	NA	0.0016	99.9
3	Oct. 25th	2,000	0	5	2.47	1.28	99.9	<0.0050	NA	0.0013	~100
4	Nov. 3rd	2,000	1	0	2.66	1.38	99.9	0.0264	97.4	<0.0005 ^c	NA
5	Nov. 4th	2,000	5	0	2.10	1.09	~100	0.0050	99.9	<0.0005	NA
6	Nov. 5th	2,000	10	0	2.76	1.44	99.9	0.0238	99.8	<0.0005	NA
7	Nov. 6th	2,000	5	1	3.82	1.99	99.9	0.0114	99.8	0.0026	99.7
8	Nov. 7th	2,000	1	5	3.26	1.69	99.9	0.0074	99.3	0.0015	~100
9	Nov. 11th	2,000	10	2	12.20	6.34	99.7	<0.0050	~100	0.0016	99.9
10	Nov. 13th	4,000	10	2	5.27	2.74	99.9	<0.0050	~100	0.0010	~100
11	Nov. 14th	6,000	10	2	10.30	5.36	99.9	<0.0050	~100	0.0012	99.9
12	Nov. 15th	8,000	10	2	8.80	4.58	99.9	<0.005	99.95	0.0020	99.9
13	Nov. 16th	10,000	10	2	18.40	9.57	99.9	<0.005	99.95	0.0050	99.8

^aTDS in the permeate water was calculated by '0.53*Conductivity'. The correlation factor 0.53 was determined by experiment.

^b0.0050 mg/L is the instrument detection limit of Fe.

^c0.0005 mg/L is the instrument detection limit of Mn.

^dNA, not applicable.

was not merely from the feed water. Metal fittings installed in the system could also be the source of iron in the feed and permeate water.

Permeate with less than 10 mg/L TDS was obtained in the tests. More than 99.7% salt rejection rate was achieved. Permeate TDS results were all below 2 mg/L in the first nine tests while relatively higher permeate TDS results were obtained in the last five tests. The ninth test with the second highest permeate TDS was conducted after a 4 d operation interval. This is in accordance with the phenomenon observed in the first experimental phase, where the ninth test conducted after a 5-d interval (Fig. 3) showed the highest permeate TDS. It suggests that intermittent operation could be the cause of permeate deterioration. Zaragoza et al. [30] have reported a similar phenomenon where anomalously high conductivity was observed at the start of daily operation. It was explained that during the discontinuous period salt deposited and penetrated the membrane pore thus affecting the initial distillate quality. Besides, salt deposition caused by the dry-out of the membrane during the intermittent operation has also been confirmed in another study to be responsible for permeate deterioration during long-term operations of solar MD systems [31]. On daily operation basis, the salt deposit could be washed out with the production of distillate. Thus, in this study, the daily production could affect the permeate TDS as only daily overall permeate samples were measured. As shown in Fig. 7, among the last five tests, the 10th test with feed TDS of 4,000 mg/L showed the lowest permeate TDS while having the highest daily production. Slightly higher permeate TDS was obtained in test 11 than in test 12 while in contrast the daily production in test 12 was higher than that in test 11. The highest permeate TDS was obtained in the last test with 10,000 mg/L TDS

feed. The increased levels of permeate TDS indicated that microleakage of membrane had taken place. Nevertheless, the permeate water was still of very good quality.

3.2.2. Daily performance of the upgraded SVMd system

Highest daily permeate water production (5.00 L) was obtained on November 5th (Test 6). The daily performance of the SVMd system on that day is presented in Fig. 8. The membrane feed temperature versus permeate pressure relationship is shown in Fig. 9.

Effective solar radiation (>400 W/m²) was obtained between 9:30 and 16:30 at the SVMd system location. It

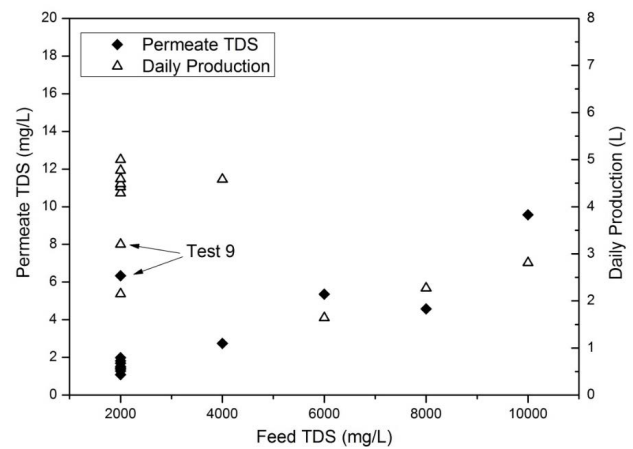


Fig. 7. Variation of permeate water TDS with different feed water salt concentrations (Phase II).

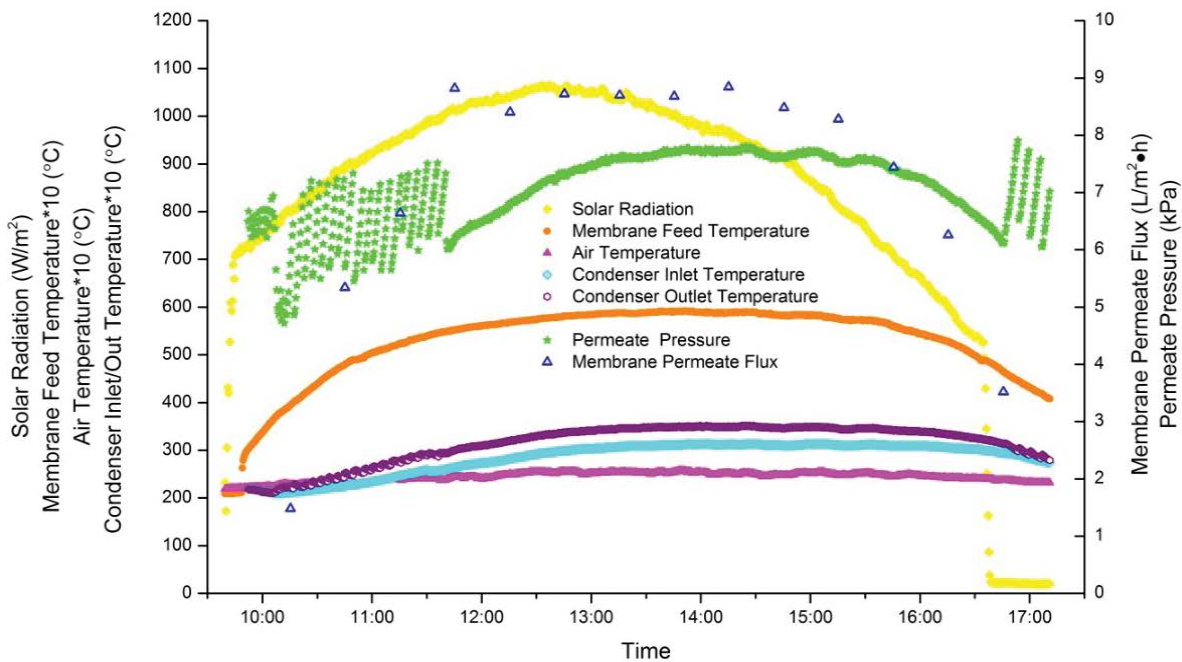


Fig. 8. Performance of the SVMd on November 5th, 2016. Variation of solar radiation, W/m²; air temperature, °C; membrane feed temperature, °C; condenser inlet temperature, °C; condenser outlet temperature, °C; permeate pressure, kPa and membrane permeate flux, L/m²·h.

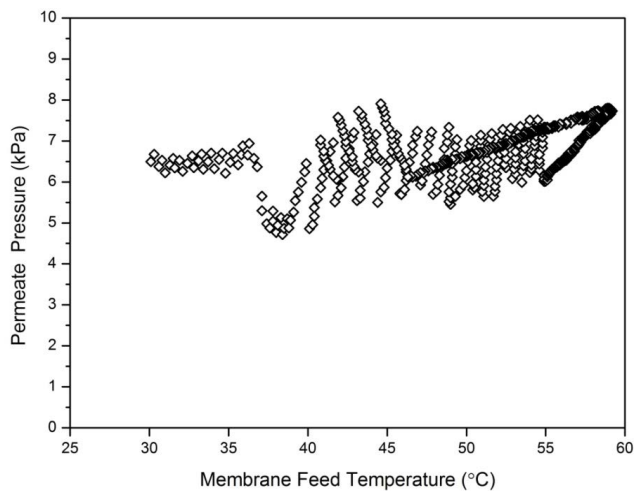


Fig. 9. Variation of permeate pressure with the change of membrane feed temperature (November 5th).

reached the peak ($1,060 \text{ W/m}^2$) at around 13:00. Membrane feed temperature increased gradually and reached the highest temperature 59.2°C at around 14:00. Similar to the phenomenon shown in Fig. 4 in Phase I, gradual increase in condenser inlet cooling water temperature (from 22.0°C to 31.3°C) was also observed here. However, the temperature differences between the condenser inlet and outlet cooling water temperature during high flux period (from 11:30 to 15:00) were much smaller ($3.5\text{--}3.9^\circ\text{C}$) compared with Phase I. This is because a much higher cooling water flow rate was applied after the installation of new condenser and the higher capacity circulation pump. Compared with the performance on September 19th (Fig. 4), much higher solar radiation was available as an energy source while in contrast much lower membrane feed temperature was obtained. This is due to the enhanced membrane permeate flux which took away more thermal energy from the hot water storage tank. The highest average flux was $8.84 \text{ L/m}^2\cdot\text{h}$ which occurred between 14:00 and 14:30. The corresponding average membrane feed temperature and permeate pressure were 58.8°C and 7.74 kPa , respectively. The peak flux was 76.1% higher than that obtained on September 19th in Phase I. The major reason for the enhanced permeate flux was the much lower permeate side pressure maintained during the operation. As shown in Fig. 8, the permeate pressure was relatively higher ($7\text{--}8 \text{ kPa}$) in the afternoon between 12:00 and 16:00 when higher membrane feed temperature ($50\text{--}60^\circ\text{C}$) was obtained. However the change was much milder compared with Phase I. Besides, the pressure fluctuations were quite sharp before 12:00 and after 16:30. This phenomenon was mainly caused by the poor arrangement of permeate side pipeline which could not drain the permeate water effectively. The vacuum efficiency was significantly affected by the temporary accumulation of permeate water in the pipeline. As shown in Fig. 9, though not very stable, the permeate pressure only varied between 5 and 8 kPa while in Phase I (Fig. 5) it was in the range of 5–25 kPa. It could be concluded that, after the installation of the new condenser and circulation pump, the condensation efficiency was significantly

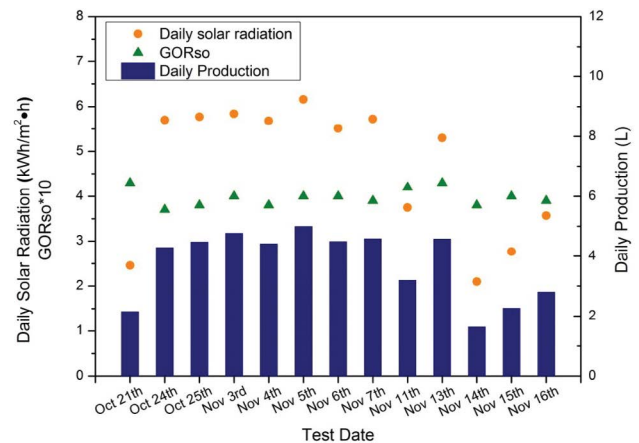


Fig. 10. Daily solar radiation, permeate production and thermal efficiency at different test days (Phase II).

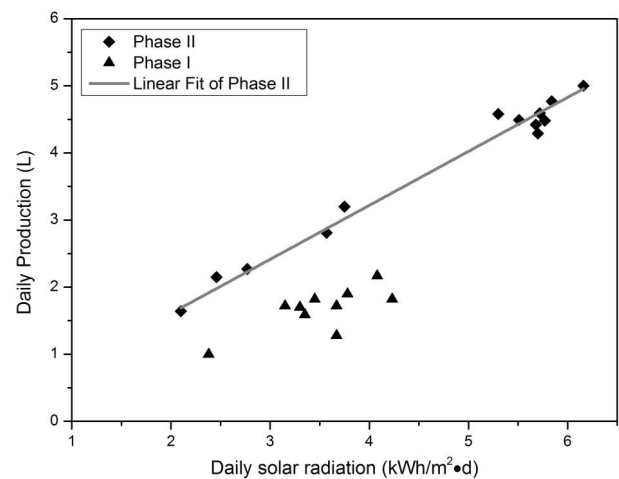


Fig. 11. Variation of daily permeate water production with the change of daily solar radiation.

enhanced and consequently the effect of produced vapour on the permeate pressure was largely reduced.

3.2.3. Production and thermal efficiency of the upgraded SVMMD system

As shown in Fig. 10, the daily production of the system during all the tests was in the range of 2.15–5.00 L. This is more than twice the production in Phase I. The high productivity could be partly due to the increased daily solar radiation as the test days were during the start of summer. However, the production was still notably higher in Phase II with the same levels of solar radiation (Fig. 11). The thermal efficiency of the system was relatively stable in different weather conditions with GOR_{so} being around 0.40, much higher than that in Phase I. This suggests that the overall thermal efficiency of the SVMMD system is significantly enhanced by improving the condensation performance of the VMD system. Meanwhile, with the relatively stable thermal efficiency, proportional relationship was shown between daily production and daily solar radiation in Phase II (Fig. 11).

4. Conclusion

The feasibility of producing potable water from BGW containing excess amounts of fluoride, iron and manganese with a three loop SVMD system has been demonstrated in this study. Tests with different feed water salinity and fluoride, iron and manganese concentrations were conducted under real weather conditions. High quality permeate water with TDS of less than 10 mg/L was produced from the SVMD system. More than 99.7% salt rejection rate was achieved in the tests. Fluoride was not detected in any of the permeate water samples while iron and manganese concentrations were all below the WHO drinking water guideline limits. The daily permeate water production in Phase I of the study was in the range of 1.00–2.17 L. The overall thermal efficiency (represented by GOR_{so}) of the SVMD system was in the range of 0.17–0.27. It was observed that the permeate pressure increased almost linearly with the membrane feed temperature which negatively affected the permeate flux. Poor condensation performance was found to be the major reason for this phenomenon. By upgrading the condensation system, much lower permeate pressure could be maintained during the operation. The membrane permeate flux was significantly enhanced. Almost twice the daily production (2.15–5.00 L) was obtained in Phase II after the upgrade compared with Phase I. Much higher GOR_{so} (around 0.40) was achieved.

Despite the improvement, the efficiency and production of this experimental system is still very low. Future studies should focus on enhancing the thermal efficiency of the system by using a more efficient membrane module, by further optimization of the condensation cycle or solar thermal system. Besides, the reliability of the SVMD system in treating BGW in the long term needs to be further demonstrated.

Acknowledgements

The authors wish to thank China Scholarship Council and University of Wollongong for their financial support towards a postgraduate scholarship to the first author. The authors are also thankful to the great help from the technical officers in the University of Wollongong, namely Dr. Ling Tie, Mr. Andrew Scobie and Mr. Peter Ihnat for their technical support in the experimentation of this study.

Symbols

A_a	–	aperture area of the solar collector, m ²
C_f	–	concentration of impurities (TDS, fluoride, Iron or manganese) in the feed solution, mg/L
C_p	–	concentration of impurities (TDS, fluoride, Iron or manganese) in the permeate, mg/L
G	–	daily solar radiation, kWh/m ² •d
GOR _{so}	–	energy ratio of total latent heat of produced distillate to the total incident solar energy
ΔH_v	–	latent heat for evaporation, kJ/kg
m_d	–	daily distillate mass production, kg/d
R	–	salt rejection rate or contaminants (fluoride, Iron or manganese) removal efficiency

References

[1] UN-Water, Water Scarcity Factsheet, The UN Water Organization, Geneva, Switzerland, 2013.

[2] A.H. Haidari, B. Blankert, H. Timmer, S.G.J. Heijman, W.G.J. van der Meer, PURO: a unique RO-design for brackish groundwater treatment, *Desalination*, 403 (2017) 208–216.

[3] R.M. Buono, K.R. Zodrow, P.J.J. Alvarez, Q. Li, Brackish Groundwater: Current Status and Potential Benefits for Water Management, Rice University's Baker Institute for Public Policy, Houston, Texas, US, April 11, 2016.

[4] J. Valdes-Abellan, L. Candela, J. Jiménez-Martínez, J.M. Saval-Pérez, Brackish groundwater desalination by reverse osmosis in Southeastern Spain. Presence of emerging contaminants and potential impacts on soil-aquifer media, *Desal. Wat. Treat.*, 51 (2013) 2431–2444.

[5] U. Yermiyahu, A. Tal, A. Ben-Gal, A. Bar-Tal, J. Tarchitzky, O. Lahav, Rethinking desalinated water quality and agriculture, *Science*, 318 (2007) 920–921.

[6] P.J. Stuyfzand, K.J. Raat, Benefits and hurdles of using brackish groundwater as a drinking water source in the Netherlands, *Hydrogeo. J.*, 18 (2010) 117–130.

[7] NSW Water Works, Brackish Groundwater: A Viable Community Water Supply Option, The National Water Commission, Australian Government, Canberra, 2011, pp. 1–81.

[8] WHO, Guidelines for Drinking-Water Quality, World Health Organization, Geneva, Switzerland, 2011.

[9] J.S. Stanton, D.W. Anning, C.J. Brown, R.B. Moore, V.L. McGuire, S.L. Qi, A.C. Harris, K.F. Dennehy, P.B. McMahon, J.R. Degnan, Brackish Groundwater in the United States, US Geological Survey, Reston, Virginia, US, 2017.

[10] M. Amini, K. Mueller, K.C. Abbaspour, T. Rosenberg, M. Afyuni, K.N. Möller, M. Sarr, C.A. Johnson, Statistical modeling of global geogenic fluoride contamination in groundwaters, *Environ. Sci. Technol.*, 42 (2008) 3662–3668.

[11] M. Mohapatra, S. Anand, B.K. Mishra, D.E. Giles, P. Singh, Review of fluoride removal from drinking water, *J. Environ. Manage.*, 91 (2009) 67–77.

[12] S. Yarlagadda, V.G. Gude, L.M. Camacho, S. Pinappu, S. Deng, Potable water recovery from As, U, and F contaminated ground waters by direct contact membrane distillation process, *J. Hazard. Mater.*, 192 (2011) 1388–1394.

[13] M. Ahmad, Iron and Manganese Removal from Groundwater, Geochemical Modeling of the Vyredox Method, Department of Geosciences, University of Oslo, Norway, 2012.

[14] S. Chaturvedi, P.N. Dave, Removal of iron for safe drinking water, *Desalination*, 303 (2012) 1–11.

[15] A. Alkhubiri, N. Darwish, N. Hilal, Membrane distillation: a comprehensive review, *Desalination*, 287 (2012) 2–18.

[16] P. Wang, T.-S. Chung, Recent advances in membrane distillation processes: membrane development, configuration design and application exploring, *J. Membr. Sci.*, 474 (2015) 39–56.

[17] S. Gabsi, N. Frikha, B. Chaouachi, Performance of a solar vacuum membrane distillation pilot plant, for seawater desalination in Mahares, Tunisia, *Int. J. Water Resour. Arid Environ.*, 2 (2013) 213–217.

[18] R.G. Raluy, R. Schwantes, V.J. Subiela, B. Peñate, G. Melián, J.R. Betancort, Operational experience of a solar membrane distillation demonstration plant in Pozo Izquierdo-Gran Canaria Island (Spain), *Desalination*, 290 (2012) 1–13.

[19] A. Chafidz, S. Al-Zahrani, M.N. Al-Otaibi, C.F. Hoong, T.F. Lai, M. Prabu, Portable and integrated solar-driven desalination system using membrane distillation for arid remote areas in Saudi Arabia, *Desalination*, 345 (2014) 36–49.

[20] Y. Zhang, M. Sivakumar, S. Yang, K. Enever, M. Ramezani-pour, Application of solar energy in water treatment processes: a review, *Desalination*, 428 (2018) 116–145.

[21] L.M. Camacho, L. Dumée, J. Zhang, J.-d. Li, M. Duke, J. Gomez, S. Gray, Advances in membrane distillation for water desalination and purification applications, *Water*, 5 (2013) 94–196.

[22] D. Hou, J. Wang, C. Zhao, B. Wang, Z. Luan, X. Sun, Fluoride removal from brackish groundwater by direct contact membrane distillation, *J. Environ. Sci. China*, 22 (2010) 1860–1867.

[23] L.J. Banasiak, T.W. Kruttschnitt, A.I. Schäfer, Desalination using electro dialysis as a function of voltage and salt concentration, *Desalination*, 205 (2007) 38–46.

- [24] L.J. Banasiak, A.I. Schäfer, Removal of inorganic trace contaminants by electro dialysis in a remote Australian community, *Desalination*, 248 (2009) 48–57.
- [25] M.A.M. Sahli, S. Annouar, M. Tahaikt, M. Mountadar, A. Soufiane, A. Elmidaoui, Fluoride removal for underground brackish water by adsorption on the natural chitosan and by electro dialysis, *Desalination*, 212 (2007) 37–45.
- [26] A.I. Schäfer, B.S. Richards, Testing of a hybrid membrane system for groundwater desalination in an Australian national park, *Desalination*, 183 (2005) 55–62.
- [27] M. Tahaikt, I. Achary, M.A.M. Sahli, Z. Amor, M. Taky, A. Alami, A. Boughriba, M. Hafs, A. Elmidaoui, Defluoridation of Moroccan groundwater by electro dialysis: continuous operation, *Desalination*, 189 (2006) 215–220.
- [28] K. Walha, R.B. Amar, L. Firdaous, F. Quéméneur, P. Jaouen, Brackish groundwater treatment by nanofiltration, reverse osmosis and electro dialysis in Tunisia: performance and cost comparison, *Desalination*, 207 (2007) 95–106.
- [29] A.K. Yadav, C.P. Kaushik, A.K. Haritash, A. Kansal, N. Rani, Defluoridation of groundwater using brick powder as an adsorbent, *J. Hazard. Mater.*, 128 (2006) 289–293.
- [30] G. Zaragoza, A. Ruiz-Aguirre, E. Guillén-Burrieza, Efficiency in the use of solar thermal energy of small membrane desalination systems for decentralized water production, *Appl. Energy*, 130 (2014) 491–499.
- [31] E. Guillén-Burrieza, R. Thomas, B. Mansoor, D. Johnson, N. Hilal, H. Arafat, Effect of dry-out on the fouling of PVDF and PTFE membranes under conditions simulating intermittent seawater membrane distillation (SWMD), *J. Membr. Sci.*, 438 (2013) 126–139.